

A Persistent-State Dataflow Accelerator for Memory-Bound Linear Attention Decode on FPGA

Neelesh Gupta*, Peter Wang*, Rajgopal Kannan† and Viktor K. Prasanna*

*University of Southern California, USA

†DEVCOM Army Research Office, USA

Email: {neeshg, plwang, prasanna}@usc.edu, rajgopal.kannan.civ@army.mil

Abstract—Gated DeltaNet (GDN) is a linear attention mechanism that replaces the growing KV cache with a fixed-size recurrent state. Hybrid LLMs like Qwen3-Next use 75% GDN layers and achieve competitive accuracy to attention-only models. However, at batch-1, GDN decode is memory-bound on GPUs since the full recurrent state must be round-tripped through HBM every token. We show that this bottleneck is architectural, not algorithmic, as all subquadratic sequence models exhibit arithmetic intensities below 1 FLOP/B at decode time, making them *more* memory-bound than standard Transformers. We present an FPGA accelerator that eliminates this bottleneck by holding the full 2 MB recurrent state persistently in on-chip BRAM, converting the workload from memory-bound to compute-bound. Our design fuses the GDN recurrence into a five-phase pipelined datapath that performs only one read and one write pass over each state matrix per token, exploits Grouped Value Attention for paired-head parallelism, and overlaps preparation, computation, and output storage via dataflow pipelining. We explore four design points on an AMD Alveo U55C using Vitis HLS, varying head-level parallelism from 2 to 16 value-heads per iteration. Our fastest configuration achieves 63 μ s per token, 4.5 \times faster than the GPU reference on NVIDIA H100 PCIe. Post-implementation power analysis reports 9.96 W on-chip, yielding up to 60 \times greater energy efficiency per token decoded.

Index Terms—FPGA Accelerator, Linear Attention, Gated DeltaNet, LLM Decode, Dataflow Architecture

I. INTRODUCTION

Large language models (LLMs) have become central to a wide range of applications, from conversational assistants to code generation and scientific reasoning. However, their deployment is constrained by the cost of inference, which is dominated by two bottlenecks: the arithmetic cost of matrix multiplications and the memory cost of maintaining per-layer context. In standard Transformer architectures [1], the key-value (KV) cache grows linearly with sequence length, consuming increasing amounts of accelerator memory as conversations or documents grow longer.

To address these scaling limitations, subquadratic sequence models [3]–[5] replace softmax attention with fixed-size recurrent state, reducing per-layer memory from $O(n)$ to $O(1)$ in sequence length. Gated DeltaNet (GDN) [2] combines selective gating with an error-correcting delta rule and has been adopted by production-scale architectures: Qwen3-Next [6] stacks three GDN layers for every one softmax attention layer, making GDN decode the dominant per-token primitive.

Critically, while LLM decode is broadly memory-bound [7]–[14], subquadratic architectures are *more* so than

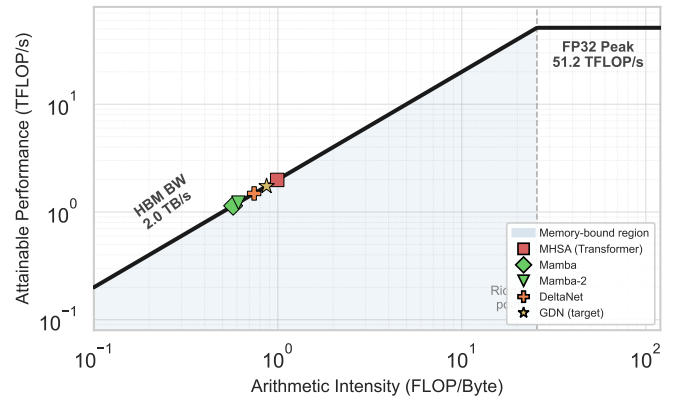


Fig. 1. Batch-1 decode arithmetic intensity on the H100 FP32 roofline. All architectures fall deep in the memory-bound regime. MHA Transformers [1] achieve an arithmetic intensity near 1 FLOP/B whereas subquadratic models (GDN [2], DeltaNet [3], Mamba [4], Mamba-2 [5]) fall well below 1 FLOP/B.

standard attention (Figure 1). MHA decode with grouped-query attention (GQA) achieves an arithmetic intensity near 1 FLOP/B, whereas recurrent models like GDN fall below: each layer must read and write its *entire* fixed-size state matrix every token, yielding only ~ 0.87 FLOP/B—well below the H100’s ridge point of 25.6 FLOP/B. Optimized kernels [15] reduce software overhead but cannot eliminate the fundamental HBM round-trip.

We observe that the full 2 MB GDN state fits in modern FPGA on-chip BRAM. By holding it persistently across kernel invocations, we eliminate the off-chip bottleneck entirely, converting the workload from memory-bound to compute-bound. We present a dataflow FPGA accelerator that exploits this insight. Our contributions are as follows:

- We propose the first FPGA accelerator for autoregressive Gated DeltaNet decode, holding the full 2 MB recurrent state persistently in on-chip BRAM to eliminate off-chip memory round-trips that limit batch-1 GPU performance.
- We fuse the GDN recurrence into a five-phase tiled datapath that performs only one read pass and one write pass over each state matrix per token, halving the naive state-access cost through an algebraic restructuring of the output computation.
- We exploit Grouped Value Attention structure to share query/key datapaths across pairs of values, scaling head-

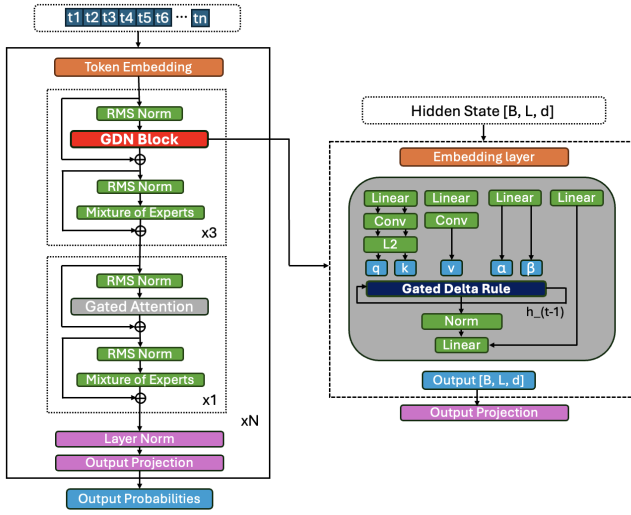


Fig. 2. Qwen3-Next [6] hybrid architecture. GDN layers (3:1 ratio) replace softmax attention with fixed-size recurrent state, making GDN decode the dominant per-token primitive.

level parallelism without increasing pipeline interval.

- We evaluate four configurations on an Alveo U55C, achieving up to $4.5\times$ lower latency than an H100 GPU. Post-implementation power analysis measures 9.96 W on-chip, yielding up to $60\times$ greater energy efficiency.

II. BACKGROUND

A. Qwen3-Next and Hybrid LLM Architectures

Next-generation LLMs increasingly adopt hybrid architectures that interleave full softmax attention layers with sub-quadratic alternatives. Qwen3-Next [6] uses a 3:1 ratio of Gated DeltaNet [2] layers to full-attention layers (Figure 2). Each GDN layer replaces the growing KV-cache with a fixed-size recurrent state matrix $S \in \mathbb{R}^{d \times d}$ ($d=128$), reducing per-layer memory from $O(n)$ to $O(1)$ in sequence length. In the Qwen3-Next configuration, each layer has $h_q = h_k = 16$ query/key heads and $h_v = 32$ value heads arranged in a 2:1 Grouped Value Attention (GVA) ratio: every query/key pair serves two value-heads that maintain independent state matrices but share the query and key vectors.

B. Prefill vs. Decode

LLM inference proceeds in two phases. During *prefill*, the model processes the full input prompt in parallel, and the GDN state matrices can be computed via efficient chunkwise parallel algorithms [3]. During *decode*, the model generates one token at a time autoregressively. Each decode step must read the current state, compute a single-token update, write the new state, and produce one output vector per head. At batch 1 this workload is extremely small (~ 4.2 M FLOPs) relative to the state that must be accessed (32 matrices of 128×128 floats = 2 MB). On GPU, this means decode is dominated by the cost of moving state through the memory hierarchy rather than by arithmetic—a classic memory-bandwidth bottleneck.

TABLE I
PLATFORM SPECIFICATIONS

	NVIDIA H100 PCIe	AMD Alveo U55C
Technology	TSMC 4N	TSMC 16 nm
FP32 peak	51 TFLOP/s	~ 2.7 TFLOP/s ^a
Memory BW	2.0 TB/s (HBM3)	460 GB/s (HBM2e)
On-chip memory	50 MB (L2 cache)	17.6 MB (BRAM)
BRAM blocks	—	$4,032 \times \text{BRAM}_{18\text{K}}$
DSP slices	—	$9,024 \times \text{DSP48E2}$
Board TDP	350 W	150 W

^a9,024 DSPs \times 300 MHz; effective throughput is datapath-dependent.

C. Gated DeltaNet Recurrence

Gated DeltaNet [2] combines the selective gating of Mamba2 [5] with the *delta rule* from DeltaNet [3]. The delta rule originates from associative memory: the state matrix S acts as a key-value store where $S^\top k$ retrieves the value currently associated with key k . Rather than blindly overwriting this association, the delta rule computes the prediction error $v - S^\top k$ and updates S proportionally, analogous to the Widrow–Hoff learning rule. This error-correcting mechanism allows the model to update stored associations incrementally without catastrophic overwriting.

For a single value-head h with state $S_{t-1} \in \mathbb{R}^{d \times d}$, the decode-step recurrence is:

$$r_t = S_{t-1}^\top k_t \quad (\text{retrieval}) \quad (1)$$

$$\Delta v_t = \beta_t (v_t - r_t) \quad (\text{delta correction}) \quad (2)$$

$$S_t = g_t \cdot S_{t-1} + k_t \Delta v_t^\top \quad (\text{state update}) \quad (3)$$

$$o_t = \frac{1}{\sqrt{d}} S_t^\top q_t \quad (\text{output}) \quad (4)$$

where $q_t, k_t \in \mathbb{R}^d$ are query and key vectors, $v_t \in \mathbb{R}^d$ is the value vector, and the scalar gates are:

$$g_t = \exp(-\sigma(\alpha_t) \cdot e^{A_{\log}} \cdot \text{softplus}(dt_{\text{bias}})) \quad (5)$$

$$\beta_t = \sigma(b_t) \quad (6)$$

Here A_{\log} and dt_{bias} are learned per-head parameters, while α_t and b_t are token-dependent inputs.

III. PERFORMANCE MODEL

A. Problem Formulation

Table I summarizes the two platforms we compare. The key asymmetry is on-chip memory *type*: the H100’s 50 MB L2 is a hardware-managed cache with no guarantee of persistence across kernel invocations, so the 2 MB GDN state must be round-tripped through HBM every token. The U55C’s 17.6 MB of BRAM, by contrast, is software-managed scratchpad that retains data indefinitely across invocations.

A single GDN decode step must update $h_v=32$ persistent state matrices $S^{(h)} \in \mathbb{R}^{d \times d}$ ($d=128$, FP32) and produce an output vector from per-token inputs. The aggregate state totals $h_v \cdot d^2 \cdot w = 2$ MB ($w=4$ bytes for FP32), while the per-token compute is only ~ 4.2 M FLOPs. Our design objective is to minimize the per-token decode latency:

$$\min_{H_{\text{iter}}} L = \frac{h_v}{H_{\text{iter}}} \cdot T_{\text{iter}} + T_{\text{load}} \quad (7)$$

Algorithm 1 Standard GDN Decode Step (Single Head)

Require: $q, k, v \in \mathbb{R}^d$, state $S \in \mathbb{R}^{d \times d}$, gates $g, \beta \in \mathbb{R}$ **Ensure:** output $o \in \mathbb{R}^d$, updated state S

- 1: $r \leftarrow S^\top k$ {Retrieval: read pass 1}
 - 2: $\Delta v \leftarrow \beta \cdot (v - r)$ {Delta correction}
 - 3: $S \leftarrow g \cdot S + k \Delta v^\top$ {State update: read+write pass 2}
 - 4: $o \leftarrow \frac{1}{\sqrt{d}} S^\top q$ {Output: read pass 3}
-

subject to the on-chip memory constraint that the full state fits in BRAM and the FPGA fabric constraints that scale with parallelism:

$$h_v \cdot d^2 \cdot w \leq B_{\text{BRAM}} \quad (8)$$

$$R_k(H_{\text{iter}}) \leq R_k^{\text{max}}, \quad k \in \{\text{DSP, FF, LUT}\} \quad (9)$$

Here H_{iter} is the number of value-heads processed per dataflow iteration—the primary design knob. T_{iter} is the per-iteration pipeline interval (dominated by two passes over a $d \times d$ state matrix), and T_{load} is the one-time cost of loading per-token inputs from host memory via AXI.

Constraint (8) is the enabling precondition: if the state fits on-chip, the off-chip memory bottleneck is eliminated entirely. On the U55C, $2\text{MB} \ll 17.6\text{MB}$, so this holds comfortably. Constraint (9) bounds the compute resources that grow with H_{iter} ; as shown in Section VI, the optimal $H_{\text{iter}}=8$ stays under 25% for all resource types.

B. Baseline Cost Analysis

Algorithm 1 shows the standard sequential GDN decode step for a single value-head [2]. This naïve approach requires *three* full passes over the $d \times d$ state matrix: one for retrieval (line 1), one for state update (line 3), and one for output (line 4).

On FPGA with column parallelism P_K , each pass over a $d \times d$ matrix costs $d \times (d/P_K)$ cycles at initiation interval 1. With $d=128$ and $P_K=16$, this gives 1,024 cycles per pass. The naïve per-head cost is therefore:

$$T_{\text{head}}^{\text{naive}} = 3 \times \frac{d^2}{P_K} = 3,072 \text{ cycles} \quad (10)$$

Processing all h_v heads sequentially in groups of H_{iter} yields the naïve total: $L^{\text{naive}} = (h_v/H_{\text{iter}}) \times 3,072 + T_{\text{load}}$.

C. Latency Decomposition

We decompose T_{iter} into the sum of per-phase costs within the compute pipeline. The two state-access phases (read and write) each cost d^2/P_K cycles; the remaining phases (dot product, delta correction, output) each cost d/P_K cycles and are negligible:

$$T_{\text{iter}} \approx 2 \times \frac{d^2}{P_K} + 3 \times \frac{d}{P_K} = 2,048 + 24 = 2,072 \text{ cycles} \quad (11)$$

In practice, pipeline startup and dataflow scheduling add a small overhead, giving $T_{\text{iter}} \approx 2,106$ cycles (verified by HLS reports). The total latency model is then:

$$L = \frac{h_v}{H_{\text{iter}}} \times 2,106 + T_{\text{load}} \quad (12)$$

TABLE II

PER-TOKEN COMPUTATIONAL PROFILE ($h_v=32, d=128, \text{FP32}$)

Quantity	GPU	FPGA (ours)
Compute (FLOPs)		$\sim 4.2\text{M}$
State I/O (bytes)	4,194,304	0
Token I/O (bytes)	49,664	49,664
Total off-chip I/O	$\sim 4.24\text{MB}$	$\sim 48.5\text{KB}$
Op. intensity (FLOP/B)	~ 1.0	~ 88

Algorithm 2 Fused GDN Decode Step (Single Head)

Require: $q, k, v \in \mathbb{R}^d$, state $S \in \mathbb{R}^{d \times d}$, gates g, β **Ensure:** output $o \in \mathbb{R}^d$, updated state S

- 1: $\alpha \leftarrow q^\top k$ {1: dot product}
 - 2: **for** each row $i = 1 \dots d$ **do**
 - 3: $r_i \leftarrow \sum_j S_{ji} \cdot k_j$; $\hat{o}_i \leftarrow g \cdot \sum_j S_{ji} \cdot q_j$
 - 4: **end for**
 - 5: $\Delta v \leftarrow \beta \cdot (v - r)$ {3: delta correction}
 - 6: $o \leftarrow \frac{1}{\sqrt{d}} (\hat{o} + \alpha \cdot \Delta v)$ {4: output correction}
 - 7: **for** each row $i = 1 \dots d$ **do**
 - 8: $S_{:,i} \leftarrow g \cdot S_{:,i} + k \cdot \Delta v_i$
 - 9: **end for**
-

This reveals three levers for reducing latency: (1) eliminate one of the state-access passes to reduce T_{iter} ; (2) increase H_{iter} to reduce the number of iterations; and (3) overlap stages within each iteration via pipelining. Table II shows the precondition enabling all three: if the state fits on-chip, state I/O vanishes, making the workload compute-bound.

IV. ARCHITECTURE DESIGN

A. Persistent On-Chip State

The foundational enabler is holding the full recurrent state—32 matrices of 128×128 FP32 values totaling 2MB—permanently in BRAM across all token steps. Unlike GPU implementations that must round-trip state through HBM every token, our state persists on-chip via static HLS arrays mapped to dual-port BRAM. The host invokes the kernel once per token, passing only the $\sim 48.5\text{KB}$ of $q/k/v$ tokens and gate values via AXI. This satisfies constraint (8) and eliminates state I/O entirely.

B. Fused Five-Phase Compute Pipeline

Naïve implementation of Eqs. (1)-(4) requires three passes over the state matrix (Eq. (10)). We reduce this to two by restructuring the algebra in state update and output steps as:

$$S_t^\top q = (g \cdot S_{t-1} + k \Delta v^\top)^\top q = g \cdot S_{t-1}^\top q + (q^\top k) \Delta v \quad (13)$$

This allows us to compute the *partial output* $\hat{o} = g \cdot S_{t-1}^\top q$ in the same read pass as the retrieval $r = S_{t-1}^\top k$, then correct the output as $o = \frac{1}{\sqrt{d}} (\hat{o} + (q \cdot k) \Delta v)$ without re-reading the updated state. Algorithm 2 shows the resulting five-phase pipeline, which performs exactly **one read pass and one write pass** per state matrix, reducing T_{iter} from $\sim 3,072$ to $\sim 2,106$ cycles—a $1.46\times$ improvement.

Recurrence distance for $\Pi=1$. The tiled accumulation in Phase 1 has a loop-carried dependency on the partial-sum registers. With $128/P_K = 8$ tiles per row, the recurrence distance is 8 cycles, exceeding the FP32 fadd latency (~ 5 cycles), guaranteeing the HLS scheduler can achieve $\Pi=1$.

C. GVA-Aware Paired-Head Parallelism

The 2:1 GVA structure means each q/k pair serves $R=2$ value-heads. We exploit this by processing both v-heads of a GVA pair simultaneously: the q and k vectors are broadcast to both heads, while each head maintains its own state matrix, gate values, and accumulators. This doubles the effective compute per q/k load without duplicating q/k storage.

More broadly, all H_{iter} v-heads are processed in parallel: the innermost loops over column tiles and head indices are fully unrolled, while the outer tile loop is pipelined at $\Pi=1$. BRAM partitioning ensures conflict-free access: complete partitioning along the head dimension gives each head its own bank group, while cyclic partitioning with factor P_K along the column dimension provides P_K independent column banks per head.

D. Dataflow Pipelining

The 32 v-heads are divided into groups of H_{iter} heads processed per iteration, yielding $N_{\text{iter}} = h_v/H_{\text{iter}}$ iterations. Each iteration comprises three stages:

- 1) *Prepare*: copy relevant q/k/v slices and compute gates g_t, β_t (Eqs. (5)–(6)).
- 2) *Compute*: execute the fused five-phase pipeline over H_{iter} heads in parallel.
- 3) *Store*: write $H_{\text{iter}} \times d$ output elements to external memory via AXI.

HLS dataflow pipelining overlaps these stages: prepare for iteration $n+1$ runs concurrently with compute for iteration n and store for iteration $n-1$. The pipeline interval is determined by the slowest stage—compute at $\sim 2,105$ cycles—so the effective iteration cost is 2,106 cycles regardless of H_{iter} . The state array is structured as a 4D tensor indexed by $[iter][h][i][j]$ so that each iteration accesses a disjoint first-dimension slice, providing the HLS compiler with static proof of no inter-iteration conflicts.

E. System Overview

Figure 3 shows how the four techniques compose. AXI master interfaces load the per-token inputs into on-chip buffers (T_{load}). The dataflow loop then iterates over head groups: each iteration’s prepare stage reads from the input buffers and computes scalar gates; the compute stage executes the fused five-phase pipeline over H_{iter} heads using the persistent BRAM state; and the store stage writes outputs back via AXI. Table III summarizes the four configurations we evaluate. The predicted latency $L = N_{\text{iter}} \times 2,106 \times 3.33$ ns gives a lower bound; measured latency is higher due to $T_{\text{load}} \approx 8,800$ – $10,600$ cycles of AXI input loading. As shown in Section VI, the constant-interval assumption breaks down at $H_{\text{iter}}=16$, where pipeline inflation causes actual latency to exceed the prediction.

TABLE III
DESIGN-SPACE CONFIGURATIONS

H_{iter} (v-heads/iter)	2	4	8	16
N_{iter} (iterations)	16	8	4	2
GVA pairs/iter	1	2	4	8
Predicted L @300MHz (μs) ^a	124.2	67.7	39.4	25.3

^aAssumes constant $T_{\text{iter}} \approx 2,106$ cycles.

V. IMPLEMENTATION

A. Target Platform

We target the AMD Alveo U55C accelerator card featuring 4,032 BRAM36 blocks (~ 17.6 MB), 9,024 DSP48E2 slices, 2.73M flip-flops, and 1.30M LUTs. The design is synthesized using Vitis HLS 2025.1 with a target clock period of 3.33 ns (300 MHz).

B. HLS Optimization Strategy

The state matrices are mapped to dual-port BRAM, providing two independent access ports per bank for concurrent read and write operations across dataflow stages. Complete partitioning along the head dimension allocates each of the H_{iter} heads to its own BRAM bank group, eliminating inter-head access conflicts. Cyclic partitioning with factor $P_K=16$ along the column dimension provides the parallel read/write bandwidth required for the tiled inner loops. All tiled loops achieve an initiation interval of one cycle, verified by HLS scheduling reports. The top-level iteration loop uses dataflow pipelining to overlap the prepare, compute, and store stages across successive iterations.

All configurations are validated via C/RTL co-simulation against a golden-reference GDN decode implementation.

VI. EVALUATION

A. Experimental Setup

Model configuration. Qwen3-Next [6]-style single GDN layer with $h_q = h_k = 16$ query/key heads, $h_v = 32$ value heads, head dimension $d = 128$. All computations in FP32.

GPU baseline. NVIDIA H100 PCIe (80 GB HBM3, 2.0 TB/s, ~ 51 TFLOP/s FP32) running the official NVlabs reference implementation (PyTorch) of the GDN decode recurrence [2].¹ At batch-1 the recurrence is inherently sequential over heads: each step loads per-token inputs, executes Eqs. (1)–(4), and stores the output—the natural structure for a recurrence that admits no cross-head parallelism. Latencies averaged over 1K invocations with CUDA warm-up.

FPGA estimates. Post-synthesis cycle counts from Vitis HLS \times clock period. We report both 300 MHz (synthesis target) and 250 MHz (conservative). Vivado implementation (place-and-route) is completed for $H_{\text{iter}} \in \{2, 4\}$: $H_{\text{iter}}=2$ achieves 263 MHz (3.802 ns critical path); $H_{\text{iter}}=4$ meets post-synthesis timing (2.370 ns critical path, identical to $H_{\text{iter}}=2$) but fails routing due to congestion (88,725 unroutable signals), as the design exceeds a single SLR (Figure 6).

¹<https://github.com/NVlabs/GatedDeltaNet>

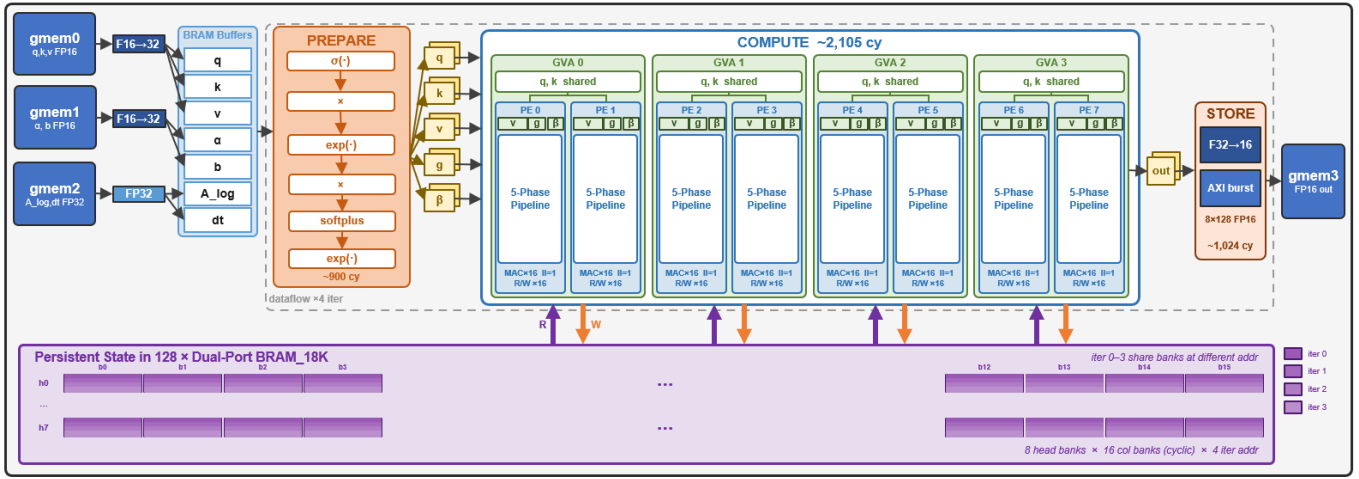


Fig. 3. System architecture for $H_{iter}=8$. Per-token inputs arrive via three AXI ports (left) and are buffered in on-chip BRAM. The prepare stage computes gates g_t, β_t . Four GVA pairs each share a q/k datapath across two PEs; each PE executes the fused five-phase pipeline with $P_K=16$ column parallelism (MAC $\times 16$, II=1). The 128 dual-port BRAM arrays (bottom) hold the persistent 2 MB state, partitioned by head and column bank, with all four iteration slices sharing the same physical banks at different addresses.

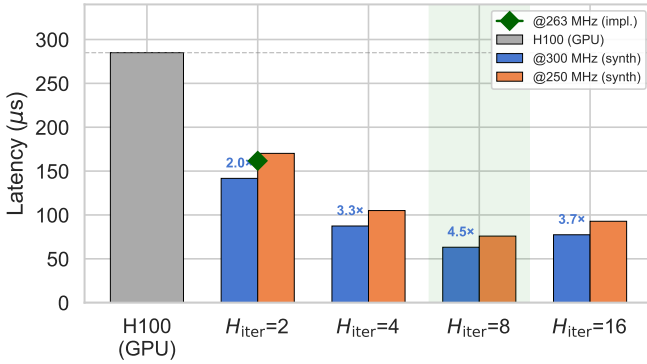


Fig. 4. Per-token latency comparison for batch-1 GDN decode. All FPGA configurations outperform the GPU baseline. $H_{iter}=8$ is optimal; $H_{iter}=16$ regresses due to pipeline interval inflation.

TABLE IV
PER-TOKEN DECODE LATENCY (μ S) AND SPEEDUP VS. GPU BASELINE

Platform	Cycles	@300 MHz	@250 MHz	Speedup
H100 (GPU)	—	—	285	1.0x
$H_{iter}=2$	42,538	141.7	170.2	2.0x
$H_{iter}=4$	26,252	87.4	105.0	3.3x
$H_{iter}=8$	18,978	63.2	75.9	4.5x
$H_{iter}=16$	23,206	77.4	92.8	3.7x

B. Latency Results

All four FPGA configurations outperform the H100 GPU baseline. For $H_{iter} \leq 8$, latency decreases with increasing parallelism, following the constant dataflow interval model: $42,538 \approx 16 \times 2,106 + 8,800$, $26,252 \approx 8 \times 2,106 + 9,400$, $18,978 \approx 4 \times 2,106 + 10,554$. The optimal is reached at $H_{iter}=8$ (4.5x speedup). At $H_{iter}=16$, however, latency increases to 77.4μ s (3.7x) because the per-iteration interval inflates from $\sim 2,106$ to $\sim 6,300$ cycles, outweighing the

TABLE V
PER-TOKEN ENERGY COMPARISON

Platform	Power	Latency	Energy/token
H100 PCIe (GPU)	350 W ^a	285 μ s	99.8 mJ
$H_{iter}=2$ (impl.)	9.96 W ^b	161.7 μ s	1.61 mJ
$H_{iter}=4$	≤ 150 W ^a	87.4 μ s	≤ 13.1 mJ
$H_{iter}=8$	≤ 150 W ^a	63.2 μ s	≤ 9.5 mJ
$H_{iter}=16$	≤ 150 W ^a	77.4 μ s	≤ 11.6 mJ

^aBoard-level TDP [16], [17] (conservative upper bound).
^bPost-implementation Vivado power estimate at 263 MHz.

reduction from 4 to 2 iterations (Section VI-E). Even at a conservative 250 MHz, $H_{iter}=8$ delivers 3.8x speedup. Post-implementation timing for $H_{iter}=2$ confirms 263 MHz is achievable, yielding 161.7 μ s latency per token.

C. Energy Efficiency

Post-implementation power analysis in Vivado reports a total on-chip power of only **9.96 W** for the placed $H_{iter}=2$ design—comprising 6.54 W dynamic (BRAM 1.67 W, DSP 0.85 W, logic 1.03 W, clocks 1.18 W, routing 1.82 W) and 3.42 W static. Table V compares per-token energy.

At 1.61 mJ per token, the implemented $H_{iter}=2$ configuration is **62x** more energy-efficient than the GPU baseline. This dramatic gap arises from two compounding factors: (1) the FPGA eliminates the HBM state round-trip, completing the workload faster; and (2) actual on-chip power at 12% resource utilization is far below the 150 W board TDP [17]. Even assuming the full 150 W board TDP, energy efficiency ranges from 7.6x to 10.5x.

D. Resource Utilization

BRAM usage is dominated by the persistent state storage (32 matrices of 128×128 FP32 values) and plateaus at 25% once the head dimension is fully partitioned ($H_{iter} \geq 4$). DSP,

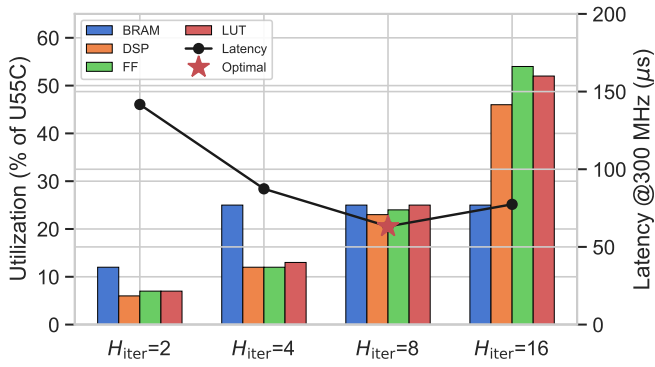


Fig. 5. FPGA resource utilization and latency across configurations. BRAM plateaus at 25%; DSP, FF, and LUT scale with H_{iter} . Latency (right axis) reaches a minimum at $H_{\text{iter}}=8$; $H_{\text{iter}}=16$ increases latency due to pipeline interval inflation despite fewer iterations.

TABLE VI
FPGA RESOURCE UTILIZATION (ALVEO U55C)

	BRAM ^a		DSP		FF	LUT
	Used	%	Used	%		
$H_{\text{iter}}=2$	523	12	570	6	7	7
$H_{\text{iter}}=4$	1,035	25	1,090	12	12	13
$H_{\text{iter}}=8$	1,035	25	2,130	23	24	25
$H_{\text{iter}}=16$	1,035	25	4,162	46	54	52

^aBRAM_18K count; 4,032 available.

FF, and LUT scale approximately linearly with H_{iter} as each additional head requires its own set of multiply-accumulate units and state-access ports. At $H_{\text{iter}}=8$, all resource types stay at or below 25%. Pushing to $H_{\text{iter}}=16$ roughly doubles compute resources (46% DSP, 54% FF, 52% LUT) while actually *increasing* latency, making $H_{\text{iter}}=8$ the optimal configuration.

E. Ablation Analysis

For $H_{\text{iter}} \in \{2, 4, 8\}$, the compute stage dominates each dataflow iteration at a near-constant $\sim 2,105$ cycles. Total latency follows the model $L \approx N_{\text{iter}} \times 2,106 + L_{\text{load}}$, where $L_{\text{load}} \approx 8,800\text{--}10,600$ cycles.

At $H_{\text{iter}}=16$, this model breaks down. The per-iteration interval inflates from $\sim 2,106$ to $\sim 6,300$ cycles because the wider datapath (16 heads unrolled) increases pipeline depth and routing pressure, raising the effective initiation interval of the tiled loops. The result is that $H_{\text{iter}}=16$ at 23,206 total cycles is *slower* than $H_{\text{iter}}=8$ at 18,978 despite having half the iterations. This identifies $H_{\text{iter}}=8$ as the optimal configuration: it minimizes latency at $4.5\times$ speedup while staying under 25% utilization for all resource types.

Physical scaling wall. Post-implementation results reinforce the synthesis trends (Figure 6). $H_{\text{iter}}=2$ places and routes within a single SLR at 263 MHz. $H_{\text{iter}}=4$ passes post-synthesis timing with an identical 2.370 ns critical path but fails routing: at 77% SLR-level BRAM and 39% LUT, the design saturates SLR0 and spills across SLR boundaries, causing 88,725 unroutable signals. This confirms that $H_{\text{iter}} \in \{8, 16\}$ would require explicit multi-SLR floorplanning or a larger

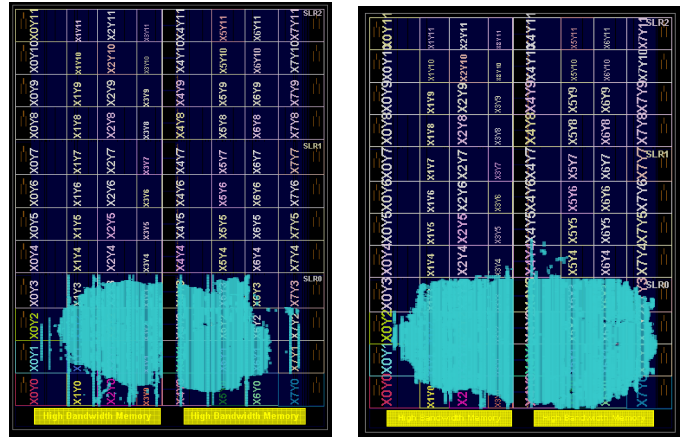


Fig. 6. Post-implementation placement on Alveo U55C. **Left:** $H_{\text{iter}}=2$ fits comfortably within SLR0 (12% BRAM, 6% DSP; 9.96 W on-chip power, 263 MHz). **Right:** $H_{\text{iter}}=4$ saturates SLR0 and spills into SLR1 (77% SLR-level BRAM, 39% LUT), causing routing failure (88,725 unroutable signals) despite meeting post-synthesis timing at 2.370 ns.

device, and that $H_{\text{iter}}=2$ represents the most implementable design point at the cost of higher latency.

VII. RELATED WORK

FPGA acceleration of Transformer-based LLMs has been explored extensively [13], [18]–[23]. DFX [18] demonstrated multi-FPGA dataflow for GPT-2 decode; Chen et al. [19] provided an analytical framework for spatial LLM acceleration; FlightLLM [20] and FlexLLM [21] target sparse Transformer and composable HLS design respectively; and LUT-LLM [13] replaces multiply-accumulate with memory-based table lookups. Since GDN is a strict superset of Mamba-2 (adding the delta rule and gating), FPGA work on Mamba is relevant: MARCA [24] introduced a reconfigurable PE array for Mamba’s mixed linear and element-wise operations, LightMamba [25] co-designs quantization with FPGA dataflow for efficient Mamba inference, and SpecMamba [26] combines speculative decoding with customized Mamba dataflow on Versal FPGAs. However, all of the above target either standard softmax attention, MLP layers, or Mamba’s simpler diagonal-state SSM recurrence. To the best of our knowledge, we are the first to accelerate the $d \times d$ matrix-state recurrence of GDN at full precision on a datacenter FPGA, targeting low-energy, production-scale LLM inference.

VIII. CONCLUSION

We presented an FPGA accelerator for Gated DeltaNet decode that eliminates the HBM state-transfer bottleneck limiting batch-1 GPU performance, achieving $4.5\times$ lower latency and over $60\times$ greater energy efficiency at under 10 W. As subquadratic models with fixed-size state increasingly replace attention layers in production LLMs, memory-boundedness becomes the dominant inference bottleneck. Future work will extend the persistent-state datapath to support prefill, mixed-precision quantization, sparse MoE routing, and co-acceleration of the remaining softmax layers to enable large-scale hybrid LLM inference on a single datacenter FPGA.

ACKNOWLEDGMENT

This work is supported by the NSF under grant numbers CNS-2009057, CCSI-2311870, CCF-1919289, and SPX-2333009.

REFERENCES

- [1] A. Vaswani, N. Shazeer, N. Parmar, J. Uszkoreit, L. Jones, A. N. Gomez, L. Kaiser, and I. Polosukhin, "Attention is all you need," *Advances in Neural Information Processing Systems*, vol. 30, 2017.
- [2] S. Yang, J. Kautz, and A. Hatamizadeh, "Gated delta networks: Improving mamba2 with delta rule," 2025. [Online]. Available: <https://arxiv.org/abs/2412.06464>
- [3] S. Yang, B. Wang, Y. Zhang, Y. Shen, and Y. Kim, "Parallelizing linear transformers with the delta rule over sequence length," *Advances in Neural Information Processing Systems*, vol. 37, 2024.
- [4] A. Gu and T. Dao, "Mamba: Linear-time sequence modeling with selective state spaces," 2024. [Online]. Available: <https://arxiv.org/abs/2312.00752>
- [5] T. Dao and A. Gu, "Transformers are ssms: Generalized models and efficient algorithms through structured state space duality," *International Conference on Machine Learning*, 2024.
- [6] QwenTeam, "Qwen3-next: Towards ultimate training & inference efficiency," 2025. [Online]. Available: <https://qwen.ai/blog?id=4074cca80393150c248e508aa62983f9cb7d27cd>
- [7] N. Shazeer, "Fast transformer decoding: One write-head is all you need," 2019. [Online]. Available: <https://arxiv.org/abs/1911.02150>
- [8] R. Pope, S. Douglas, A. Chowdhery, J. Devlin, J. Bradbury, J. Heek, K. Xiao, S. Agrawal, and J. Dean, "Efficiently scaling transformer inference," in *Proceedings of Machine Learning and Systems (MLSys)*, 2023.
- [9] Y. Leviathan, M. Kalman, and Y. Matias, "Fast inference from transformers via speculative decoding," in *International Conference on Machine Learning*, 2023.
- [10] Z. Yuan, Y. Shang, Y. Zhou, Z. Dong, Z. Zhou, C. Xue, B. Wu, Z. Li, Q. Gu, Y. J. Lee *et al.*, "LLM inference unveiled: Survey and roofline model insights," *arXiv preprint arXiv:2402.16363*, 2024.
- [11] S. Kim, C. Hooper, A. Gholami, Z. Dong, X. Li, S. Shen, M. W. Mahoney, and K. Keutzer, "SqueezeLLM: Dense-and-sparse quantization," in *International Conference on Machine Learning*, 2024.
- [12] R. Jayanth, N. Gupta, and V. Prasanna, "Benchmarking edge ai platforms for high-performance ml inference," in *2024 IEEE High Performance Extreme Computing Conference (HPEC)*, 2024, pp. 1–7.
- [13] Z. He, S. Ye, R. Ma, Y. Wang, and J. Cong, "Lut-llm: Efficient large language model inference with memory-based computations on fpgas," 2025. [Online]. Available: <https://arxiv.org/abs/2511.06174>
- [14] C. He, Y. Chen, Z. Zhao, K. Yang, B. Jiang, L. Cai, K. Chen, Z. Li, Y. Ren, Z. Zhang *et al.*, "WaferLLM: Large language model inference at wafer scale," in *USENIX Symposium on Operating Systems Design and Implementation (OSDI)*, 2025.
- [15] C. F. Chen, Z. Ye, H. Ying, Y. Chen, L. Zheng, Y. Zhang, E. Park, Y. Zheng, Z. Jia, and L. Song, "Flashinfer: Efficient and customizable attention engine for llm inference serving," *Conference on Machine Learning and Systems (MLSys)*, 2025.
- [16] NVIDIA Corporation, "NVIDIA H100 Tensor Core GPU Datasheet," 2024, tDP: 350 W (PCIe), 700 W (SXM).
- [17] AMD Xilinx, "Alveo U55C Data Center Accelerator Card Data Sheet (DS989)," 2023, maximum power: 150 W.
- [18] S. Hong, S. Moon, J. Kim, S. Lee, M. Kim, D. Lee, and J.-Y. Lee, "Dfx: A low-latency multi-fpga appliance for accelerating transformer-based text generation," in *2022 55th IEEE/ACM International Symposium on Microarchitecture (MICRO)*. IEEE, 2022, pp. 616–630.
- [19] H. Chen, J. Zhang, Y. Du, S. Xiang, Z. Yue, N. Zhang, Y. Cai, and Z. Zhang, "Understanding the potential of fpga-based spatial acceleration for large language model inference," *ACM Transactions on Reconfigurable Technology and Systems*, 2024.
- [20] S. Zeng, J. Liu, G. Dai, X. Yang, T. Fu, H. Wang, W. Ma, H. Sun, S. Li, Z. Huang, Y. Dai, J. Li, Z. Wang, R. Zhang, K. Wen, X. Ning, and Y. Wang, "Flightllm: Efficient large language model inference with a complete mapping flow on fpgas," 2024. [Online]. Available: <https://arxiv.org/abs/2401.03868>
- [21] J. Zhang, Z. He, N. Fraser, M. Blott, Y. Sun, and J. Cong, "Flexllm: Composable hls library for flexible hybrid llm accelerator design," *arXiv preprint arXiv:2601.15710*, 2026.
- [22] Y. Guan, H. Liang, N. Xu, W. Wang, S. Shi, X. Chen, G. Sun, W. Zhang, and J. Cong, "Fp-dnn: An automated framework for mapping deep neural networks onto fpgas with rtl-hls hybrid templates," in *2017 IEEE 25th Annual International Symposium on Field-Programmable Custom Computing Machines (FCCM)*. IEEE, 2017, pp. 152–159.
- [23] S. Han, J. Kang, H. Mao, Y. Hu, X. Li, Y. Li, D. Xie, H. Luo, S. Yao, Y. Wang *et al.*, "Ese: Efficient speech recognition engine with sparse lstm on fpga," *ACM/SIGDA International Symposium on Field-Programmable Gate Arrays*, pp. 75–84, 2017.
- [24] J. Li, S. Wu, Y. Zheng, J. Tang, B. Li, and J. Cong, "Marca: Mamba accelerator with reconfigurable architecture," in *Proceedings of the 43rd IEEE/ACM International Conference on Computer-Aided Design (ICCAD)*, 2024.
- [25] R. Wei, Y. Xu, X. Huang, and Z. Tan, "Lightmamba: Efficient mamba acceleration on fpga with quantization and hardware co-design," 2025. [Online]. Available: <https://arxiv.org/abs/2502.15260>
- [26] W. Wu, J. Li, Y. Zheng, Y. Huang, Z. He, and J. Cong, "Specmamba: Accelerating mamba inference on fpga with speculative decoding," 2025. [Online]. Available: <https://arxiv.org/abs/2509.19873>